ELSEVIER

Journal of Hazardous Materials B127 (2005) 156–162

Journal of Hazardous Materials

www.elsevier.com/locate/jhazmat

Dechlorination of hexachlorobenzene using ultrafine Ca–Fe composite oxides

Xiaodong Ma, Minghui Zheng*, Wenbin Liu, Yong Qian, Bing Zhang, Wenxia Liu

State Key Laboratory of Environmental Chemistry and Ecotoxicology, Research Center for Eco-Environmental Sciences, Chinese Academy of Sciences, P.O. Box 2871, Beijing 100085, China

Received 1 February 2005; received in revised form 29 June 2005; accepted 30 June 2005
Available online 2 August 2005

Abstract

Ca–Fe composite oxides with different Ca/Fe atomic ratios were synthesized by co-precipitation method and characterized by X-ray diffraction (XRD), scanning electron microscopy with elemental X-ray analysis (SEM-EDX) and inductively coupled plasma optical emission spectrometer (ICP-OES). Their dechlorination activities were evaluated using hexachlorobenzene (HCB) as a model compound. The results indicate that the dechlorination activity is related to the composition of metal oxides. Different compositions lead to the formation of different phases of Ca–Fe composite oxides. When Ca/Fe atomic ratio was 3.4, the dechlorination activity reached 97%, which was the highest in the dechlorination of HCB at 300 °C for 0.5 h. This may be related to the formation of $Ca_2Fe_2O_5$ phase and small agglomerate size of oxide crystal of about 1 μm. The effect of reaction time on HCB dechlorination and the pathway of dechlorination were investigated using the Ca–Fe composite oxide with the highest activity. It was found that hydrodechlorination took place in the destruction of HCB, the dechlorination efficiency is almost 100% after 2 h reaction. After reaction, quantitative measurement of chloride ion and qualitative analysis of $CaCO_3$ indicate besides hydrodechlorination, other degradation routes may be present. The mechanism of synergic dechlorination using Ca–Fe composite oxides was discussed.

Keywords: Dechlorination; Ca–Fe composite oxides; HCB; Co-precipitation

1. Introduction

Polychlorinated aromatic compounds are environmentally persistent chemicals, recalcitrant toward degradation, which bioaccumulate in fatty tissue and show carcinogenic and mutagenic activity, so they are a class of pollutants of special environmental concern [1]. The most extensively used treatment method involves incineration [2]. Toxic chlorinated compounds appear to be completely destroyed by high-temperature thermal oxidation; however, it is related to the release of even more toxic compounds such as chlorinated dioxins and furans. The development of a highly efficient, safe alternative technology for detoxifying organic halides has been anticipated.

Lots of technologies have been developed for the disposal of chlorinated aromatics at low temperature. They include biodegradation [3–5], photocatalytic oxidation [6,7] and catalytic hydrodechlorination [8–17]. In general, chemical methods have been by far the most studied ones. The chemical reduction of organic halides involving the replacement of halogen by hydrogen is the so-called hydrogenolysis of the carbon–halogen bond or hydrodehalogenation reaction, which is known to be promoted by noble metals of group VIII, such as Ni, Pd and Ru. Compared with traditional oxidation methods, catalytic hydrodechlorination presents the following advantages: (i) mild reaction conditions; (ii) no associated dioxin and dibenzofuran formation. However, they are not adapted to large-scale applications [18], due

* Corresponding author. Tel.: +86 10 62849172; fax: +86 10 62923563.
E-mail address: zhengmh@mail.rcees.ac.cn (M. Zheng).

0304-3894/$ – see front matter © 2005 Elsevier B.V. All rights reserved.
doi:10.1016/j.jhazmat.2005.06.034

to severe reaction conditions or the high cost. In related work, some methods have been reported with metal oxide as dechlorination reagent. Among them, some oxides were used for catalytic oxidation without metal loading [19–23], others were acted as supports for metal elements [24,25]. In seeking to find less expensive reagents for organochlorine destruction, the behavior of CaO, MgO and Fe_2O_3 has been examined [26–28], respectively. Further studies have revealed that the reaction efficiencies can be improved by the presence of a small amount of transition-metal oxide as catalyst coated on nanoparticles. Such ultrafine (nanoscale) particles of metal oxides ([Fe_2O_3]MgO, [Fe_2O_3]CaO and [V_2O_3]MgO) have been synthesized in the form of shell/core-like material [29–31]. Considering the high cost of preparation of nanocrystalline by sol–gel method and the complicated synthetic procedure, a cheaper but efficient method is expected.

In this paper, we report the preparation of ultrafine Ca–Fe composite oxides by using co-precipitation method. For evaluation of the dechlorination activity for polychlorinated aromatic compounds, hexachlorobenzene (HCB) was chosen as a model compound. It was found that at relatively low temperature (300 °C) and short time, a high dechlorination efficiency was reached.

2. Experimental

2.1. Sample preparation

The Ca–Fe composite oxide powers were synthesized with co-precipitation method. $Fe(NO_3)_3{\cdot}9H_2O$ and $Ca(NO_3)_2{\cdot}4H_2O$ (analytic reagent grade) were used as the starting materials and NaOH as the co-precipitant without further purification. The two salts mentioned above were mixed and dissolved in deionized water in quantities required. The solution was thoroughly stirred in a water bath at 50 °C. Then, 370 ml 0.5 mol/l NaOH aqueous solution was slowly added to the above solution to reduce the pH to around 9 and continued stirring for 10 min. The formed precipitate was filtered and washed with deionized water and ethanol in sequence, then dried at 120 °C for 20 h to form the precursor of metal oxides. Finally, the formed precursor was calcined in air at 600 °C to produce the ultrafine Ca–Fe composite oxides. The pure Fe_2O_3 and CaO have been synthesized with the same procedure.

2.2. Characterization

Powder X-ray diffraction (XRD) patterns of the samples were recorded using a D8-discover diffractometer under the following conditions: 40 kV, 40 mA and Cu Kα radiation. Scan speed was $6^\circ\,min^{-1}$ in the range from 20° to 60°. Diffraction peaks of crystalline phases were compared with those of standard compounds reported in the JCPDS Data File.

SEM analyses were carried out with a Hitachi-3000N electron microscope equipped with an EDX analyzer (EDAX-Genesis).

Elemental analysis was performed on an Optima 2000 DV model inductively coupled plasma optical emission spectrometer (ICP-OES). Sample solutions were prepared by dissolving the samples in dilute hydrochloric acid (1:1).

Measurement of the surface area was based on N_2 adsorption data obtained using a NOVA 4200e analyzer.

Chloride ion (Cl^{-1}) was measured potentiometrically using a pCL-1 chloride selective electrode (Shanghai Kangyi Company) with a separate reference electrode calibrated with NaCl standards.

2.3. Dechlorination of HCB

The dechlorination of HCB was carried out in a small glass tube (11 cm length, 0.4 cm i.d.). CaO–Fe_2O_3 oxide with different compositions, CaO and Fe_2O_3 were acted as dechlorination reagent (DeCR). The oxides were ground into powders of average particle size ~ 50 μm. For all reactions, 2.0 mg of HCB was mixed with 40 mg DeCR and then sealed under air atmosphere and was heated in an oven. The reaction temperature was fixed at 300 °C.

2.4. Analysis of the products

After finishing the experiments, the glass tubes were carefully crushed and subjected to extraction. Each sample was extracted with 15 ml hexane twice for 15–20 min each time in an ultrasonic extractor. Then, the solution was washed with 10 ml of water twice, and the aqueous layer and hexane layer were separated, then 10 ml of HNO_3 (10%, v/v, aqueous solution) was added to the solid residue and stirred for 15 min before the insoluble material is filtrated out and washed carefully with water (10 ml). The combined filtrate plus all water washings were used for measurement of chloride anion. The hexane layers were combined and dried with anhydrous sodium sulfate. The organic extract was used for the measurement of parent HCB remaining and lower chlorinated benzenes newly formed. The analyses of chlorobenzenes were performed by an Agilent 6890 gas chromatograph equipped with a DB-5 capillary column (30 m length, 0.25 mm i.d., 0.25 μm film thickness) and interfaced to Agilent 5973N MSD. Quantitative analyses of chlorobenzenes were performed in selected ion monitoring mode using two most abundant ions of the molecular ion clusters.

The declorination efficiency (DE, %) for initial HCB is calculated using following equation:

$$\mathrm{DE}\ (\%) = \left(1 - \frac{\sum_{i=0}^{6} i N_i}{6 N_0}\right) \times 100$$

where N_i is the molar number of chlorinated benzene containing i chlorine atoms in the molecule and N_0 is the initial molar number of HCB.

The definition used for organic chloride mineralization is as follows:

$$\text{Organic chloride mineralization (\%)} = \frac{Cl^-}{Cl_0} \times 100$$

where Cl^- is the molar number of formed chloride anion and Cl_0 is the molar number of chlorine atom from initial HCB.

3. Results and discussions

3.1. Synthesis and characterization of the DeCR

$CaO–Fe_2O_3$ metal oxides can be prepared by sol–gel method [21], which allows to obtain nanocrystalline with high surface area, but the procedure of synthesis is complicated and costly. In this study, the attention was focused on $CaO–Fe_2O_3$ oxides of different composition prepared by co-precipitation. The sample codes for all oxides prepared and the related main characteristics are reported in Table 1.

The XRD patterns of the $CaO–Fe_2O_3$ powders with different Ca/Fe atomic ratios are shown in Fig. 1. Compared with pure CaO (JCPDS file no. 40777) and α-Fe_2O_3 (JCPDS file no. 330664), the intensities of peaks of S2, S3, S4 and S5 tend to decrease, due to the formation of other phases such as $Ca_2Fe_2O_5$ (JCPDS file no. 180286), $CaFe_2O_4$ (JCPDS file no. 320168) and CaO! Fe_2O_3 (JCPDS file no. 30825).

Table 1
Main characteristics of the sample prepared using the co-precipitation method

Sample	Ca/Fe atomic ratio	Main XRD phases obtained		BET surface area ($m^2\ g^{-1}$)
S1	∞	CaO		8.8
S2	3.4	CaO	$Ca_2Fe_2O_5$	3.7
S3	1.1	CaO	$Ca_2Fe_2O_5$	27.1
S4	0.33	α-Fe_2O_3	CaO! Fe_2O_3	18.1
S5	0.17	α-Fe_2O_3	$CaFe_2O_4$	8.5
S6	0	α-Fe_2O_3		10.6

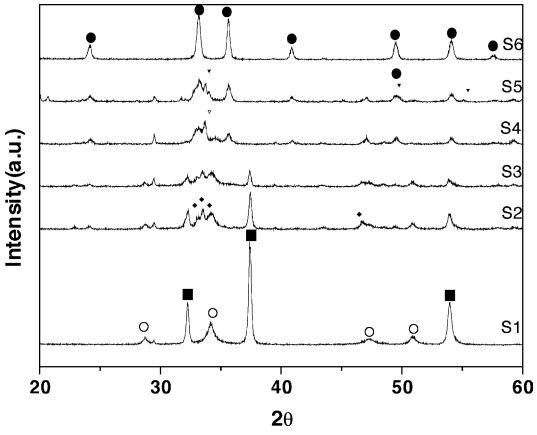

Fig. 1. XRD patterns of the $CaO–Fe_2O_3$ composite oxides of different compositions: (■) CaO; (●) α-Fe_2O_3; (◯) $Ca(OH)_2$; (♦) $Ca_2Fe_2O_5$; (▽) CaO! Fe_2O_3; (▼) $CaFe_2O_4$.

Some new diffraction peaks that are obviously different from those of calcium oxide and iron oxide are detectable in the XRD patterns. It indicates that after calcinations, composite metal oxide phase containing Fe^{3+} and Ca^{2+}cations have developed. When Ca/Fe atomic ratio is higher than 0.33, CaO phase is present, whose intensity increases with increasing Ca loading. For S2 and S3, there are no changes in phase except that the widths and intensities of diffraction peaks are different. The crystalline size of the metal oxide phase was estimated using Scherrer equation. The mean crystalline sizes of CaO are 38, 36 and 38 nm for S1, S2 and S3, respectively. When Ca/Fe atomic ratio is lower than 1.1, the CaO phase is never observed. XRD patterns show the reflections of α-Fe_2O_3 and other composite phases. The mean crystalline sizes of α-Fe_2O_3 are 29, 23 and 36 nm for S4, S5 and S6, respectively.

It is obvious that grain size of CaO tends to be small, when doped with small amounts of α-Fe_2O_3. However, the value increases again with the addition of more α-Fe_2O_3. The emergence of $Ca(OH)_2$ can be attributed to the dissociative adsorption of water.

SEM micrographs are shown in Fig. 2. All ultrafine oxide particles agglomerate into coarser ones. Among all Ca–Fe composite oxides, the powder of S2 has the smallest agglomerate size of about 1 μm. On pure α-Fe_2O_3, large particles of irregular form were observed. On pure CaO, the particle size is small and round. Among the four samples with composite phases, the higher the amount of the Fe, the more irregular and coarser the agglomerates are.

The distributions of Fe, Ca and O, on the surface of the sample, were characterized by scanning electron microscopy with elemental X-ray analysis (SEM-EDX) as shown in Fig. 3, where the diagram of S2 is the image of the whole chemical element, and the spots whose grayscales are different from the backgrounds in the other diagrams represent distributions of Fe, Ca and O, respectively. It can be found that the distributions of Fe, Ca and O were homogeneous.

3.2. Dechlorination activities for hexachlorobenzene

3.2.1. Comparison of the activities for dechlorination of HCB over the ultrafine Ca–Fe composite oxides of different compositions

The dechlorination of HCB was used to evaluate the dechlorination activities of ultrafine Ca–Fe composite oxide particles. The dechlorination reaction was investigated at 300 °C for 30 min. Each experiment was performed three times. The activities of ultrafine Ca–Fe composite oxides with different Ca/Fe atomic ratios were compared and the average results are shown in Table 2. It can be seen that the dechlorination activities of ultrafine Ca–Fe composite oxide particles follow the following order: S2 > S3 > S5 > S4. All the composite oxides exhibit higher activities than monocomponent oxides except S4. S2 and S3 have higher dechlorination activity, this may be attributed to the formation of $Ca_2Fe_2O_5$ phase.

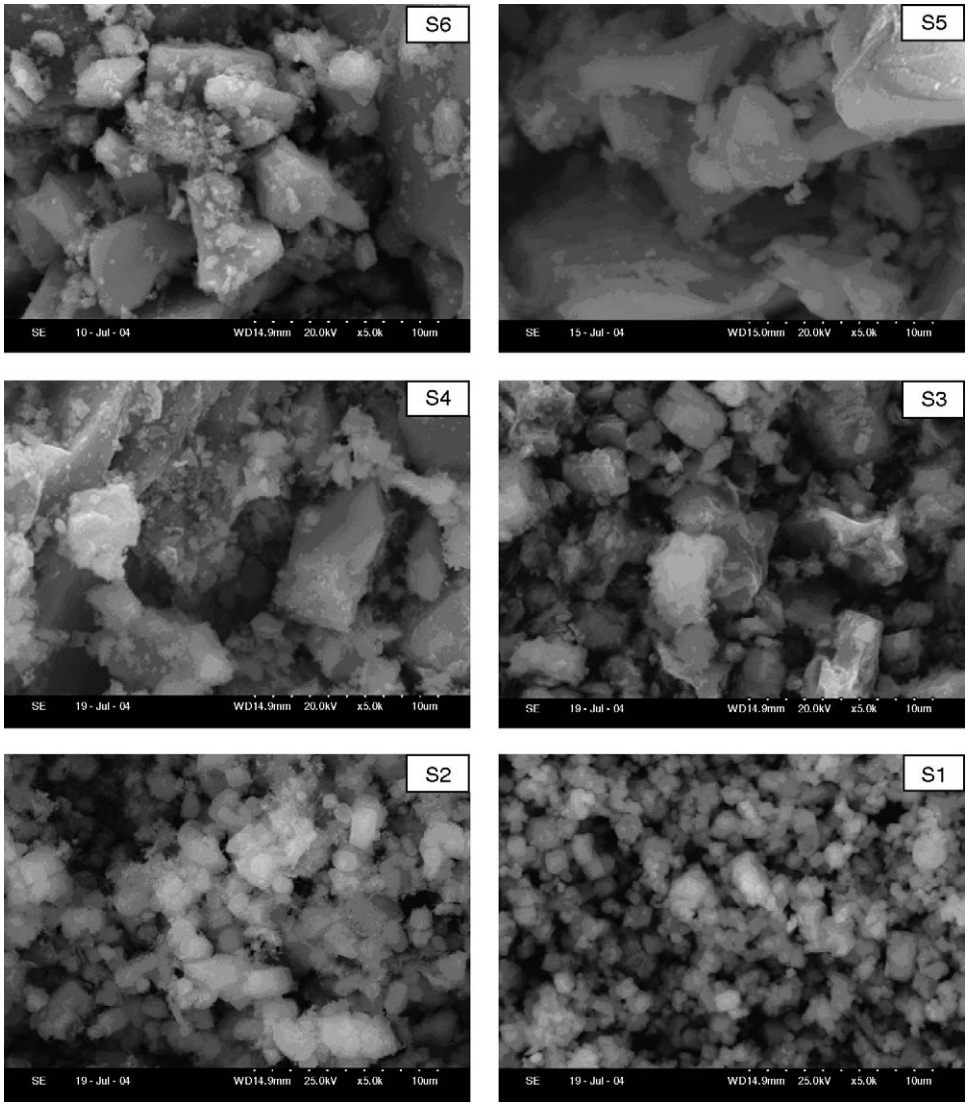

Fig. 2. SEM images of the CaO–Fe_2O_3 composite oxides of different compositions.

Comparing the physical characteristics and dechlorination activity between S2 and S3, it was found that even though S2 has smaller surface area (shown in Table 1), it has better crystallinity (shown in Fig. 1) of $Ca_2Fe_2O_5$ phase, which may lead to its better dechlorination activity. As discussed above, the smallest crystal particles and agglomerate sizes are observed in S2 with Ca/Fe = 3.4. This may be another factor affecting dechlorination activity.

3.2.2. The effect of reaction time on HCB dechlorination with S2 as DeCR

Considering S2 exhibits the highest dechlorination activity, in this study, a series of experiments with S2 were designed to determine the effect of time on HCB dechlorination in order to investigate the detailed process of declorination. The dechlorination reactions were carried out at 300 °C. The intermediates formed and the declorination efficiency in the experiments are given in Table 3.

It could be seen from Table 3 that the percentage of dechlorination increases rapidly within 5 min and reaches 67%, then increases slowly with further reaction. The value reaches about 97% at 30 min of reaction (shown in Table 2). At the last stage of the reaction, the dechlorination rate tends to decrease obviously, it takes 90 min to increase by 2% of DE.

The data of Table 3 reflect the effect of reaction time on the distribution of products obtained. It is observed that the dechlorination is deeper with increasing reaction time. Within 15 min, only PeCB is detected. After that, the formed TeCB isomers increase until 60 min. With further reaction, TrCB and DCB isomers are detected.

Decreasing orders of chlorobenzenes by amount are 1,2,3,5- > 1,2,4,5- > 1,2,3,4- for tetrachlorobenzenes (TeCB) and 1,2,4- > 1,3,5- ≈ 1,2,3- for trichlorobenzenes (TrCB); the amounts of 1,3-, 1,4- and 1,2-dichlorobenzene (DCB) are almost the same. The pathway to form 1,2,4-TrCB must be a major pathway because the highest amount of 1,2,4-TrCB

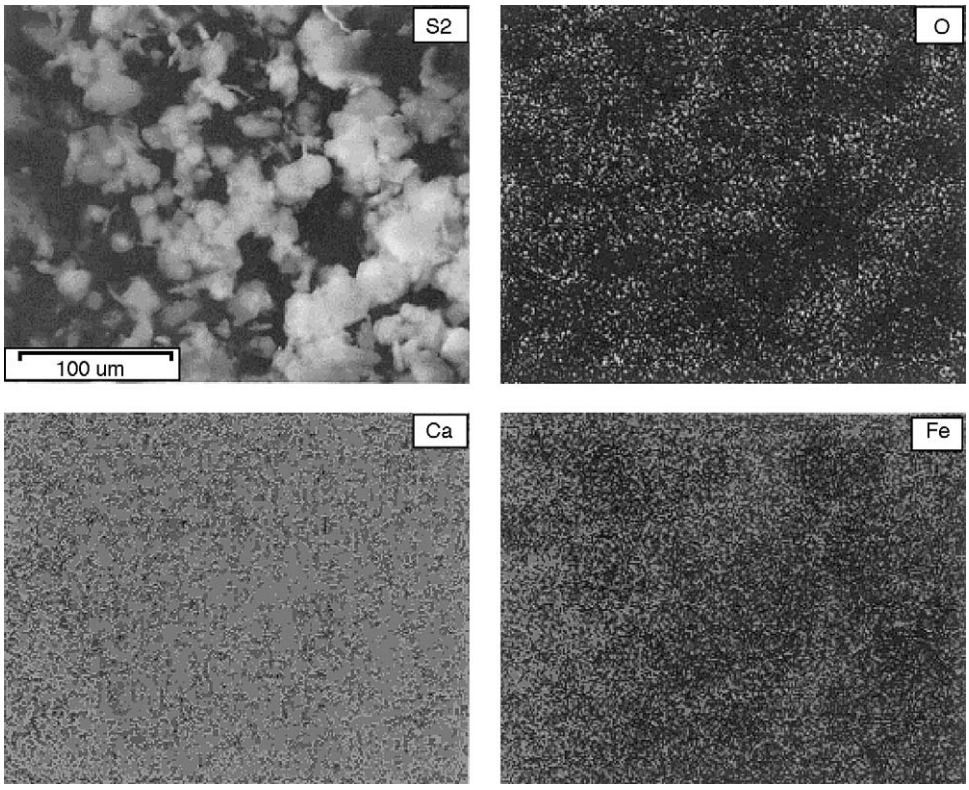

Fig. 3. SEM-EDX images of S2.

(64 nmol) is detected. All TeCB-, TrCB- and DCB-isomers are detected, showing the presence of more than one dechlorination pathway.

It is worthy to be mentioned that the intermediate products detected are in low amounts. There exists discrepancy in the material balance of the starting and dechlorinated materials. This implies besides dechlorination, another degradation process can be present.

3.2.3. Fate of chlorine and carbon atoms in the dechlorination of HCB with S2 as DeCR

To further understand if there are inorganic ions released to reach mineralization in the decomposition of HCB by S2, chloride selective electrode is utilized to monitor the levels of chloride ions after the reaction. Fig. 4 shows the extent of mineralization of organic chlorine in the 2 h of reaction time. It is found that within the first 5 min, organic chlorine is converted into inorganic chloride rapidly, the extent of mineralization is 35%. After 30 min, the value remains at 50%, and it is no distinct change as the reaction time increases. At 30 min of reaction time, comparing the dechlorination extent

Table 2
Comparison of the activities for dechlorination of HCB[a] (nmol) over the ultrafine Ca–Fe composite oxides

Chlorobenzenes	Sample					
	S1	S2	S3	S4	S5	S6
1,2,4,5-TeCB	ND[b]	20	ND	ND	ND	ND
1,2,3,5-TeCB	ND	36	ND	ND	ND	ND
1,2,3,4-TeCB	ND	14	ND	ND	ND	ND
PeCB	538	102	255	56	513	321
HCB	3764	94	782	4672	1875	3273
DE[c] (%)	40	97	86	33	67	50

[a] Initial amount of HCB was 7022.5 nmol.
[b] ND—not detected. The detection limit for TeCB, PeCB and HCB was 0.2, 0.2 and 0.1 nmol, respectively.
[c] DE—dechlorination efficiency.

Table 3
Formation of dechlorination products (nmol) during reaction process (initial amount of HCB was 7022.5 nmol)

Chlorobenzenes	Reaction time (min)			
	5	15	60	120
1,3-DCB	ND[a]	ND	ND	3
1,4-DCB	ND	ND	ND	4
1,2-DCB	ND	ND	ND	2
1,2,4-TrCB	ND	ND	18	64
1,3,5-TrCB	ND	ND	3	10
1,2,3-TrCB	ND	ND	2	7
1,2,4,5-TeCB	ND	ND	62	24
1,2,3,5-TeCB	ND	ND	69	38
1,2,3,4-TeCB	ND	ND	36	11
PeCB	69	102	152	4
HCB	2250	1043	29	3
DE[b] (%)	67	84	96	99

[a] ND—not detected. The detection limit for DCB, TrCB, TeCB, PeCB and HCB was 0.8, 0.3, 0.2, 0.2 and 0.1 nmol, respectively.
[b] DE—dechlorination efficiency.

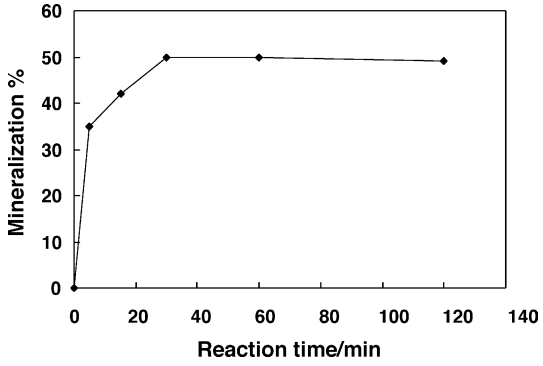

Fig. 4. Extent of mineralization (%) as a function of reaction temperature.

of HCB and the mineralization extent of organic chlorine, it can be seen that there exists larger discrepancy between the two values (97 and 48%, respectively), which indicates organochlorine atoms were only partially mineralized and were released in the forms of inorganic ions. It can be conjectured that a formation of some organochlorine compounds was taking place.

The new phase formed on the oxide after reaction was identified by X-ray diffractometer and the result was compared with JCPDS database. The XRD pattern (Fig. 5) showed that the new crystal phase formed after 30 min reaction was $CaCO_3$ (JCPDS file no. 50586). This means the C–C bond breaking of aromatic ring took place under the reaction conditions.

It implies that other organochlorine compounds may be formed though they were not detected. The formation of $CaCO_3$ can also give an explanation for the discrepancy in the material balance of the starting and dechlorinated material.

3.3. The mechanism of synergic dechlorination by Ca–Fe composite oxides

From the comparison of dechlorination activity in Table 2, it is found that among all samples, S2 with CaO and $Ca_2Fe_2O_5$ co-existed is the most active. The average amount of residual HCB is only 94 nmol, much lower than the original 7022.5 nmol, and dechlorination efficiency is about 97%. In contrast, pure CaO and Fe_2O_3 show lower activity. It is obvious the formation of $Ca_2Fe_2O_5$ exhibits a synergic effect in the dechlorination of HCB.

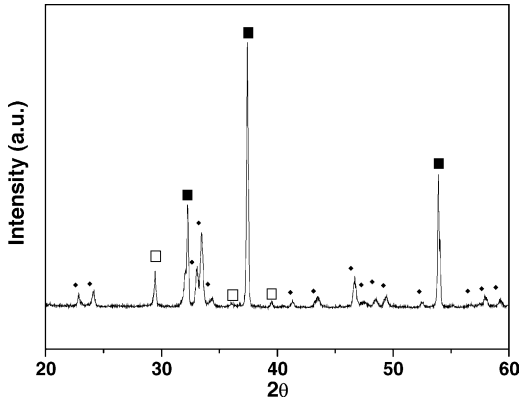

Fig. 5. XRD patterns of S2 after reaction with HCB: (■) CaO; (♦) $Ca_2Fe_2O_5$; (□) $CaCO_3$.

Previous studies have revealed that CaO could improve the decomposition of chlorinated hydrocarbons over iron oxide catalysis [20,21]. This effect is attributed to ion exchange between the CaO and $FeCl_3$, the latter being formed as a result of interaction of iron oxide with chlorinated hydrocarbons. In that case, calcium serves as a sink for chlorine ions, regenerating iron oxide. For efficient chloride ion exchange between iron and calcium in an interfacial process, good contact between the phases is necessary. The systems discussed in the previous papers [21] were composed of transition-metal oxides, such as Fe_2O_3, supported on CaO with intimate contact. In this paper, Fe and Ca are distributed homogeneously in the composite oxides. It is reasonable to assume a synergic effect based on the basic Ca–O–Fe mixtured structure, in which Ca is the adsorption center and Fe is the catalysis center. This structure is favourable for the synergic effect of the two active centers. When Ca/Fe atomic ratio is in the vicinity of 3.4, the best adsorption and catalysis capacity can be reached.

4. Conclusion

Ca–Fe composite oxide with appropriate composition was proven to possess excellent dechlorination activity at relatively low temperature. This dechlorination technique can be a promising method to detoxify polychlorinated aromatic compounds.

According to the quantitative analysis of residual HCB and lower chlorinated benzenes, the conclusion can be made that the process of hydrodechlorination exists in the reaction. The dechlorination activity could be assigned to the formation of Ca–O–Fe mixtured structure.

Acknowledgements

This study is supported by national 973 project (2003CB415006) and National Natural Science Foundation of China (20177031, 20122202).

References

[1] F. Alonso, I.P. Beletskaya, M. Yus, Metal-mediated reductive hydrodehalogenation of organic halides, Chem. Rev. 102 (2002) 4009–4091.
[2] C.C. Lee, G.L. Huffman, Innovative thermal destruction technologies, Environ. Prog. 8 (1989) 190–199.
[3] B.V. Chang, C.J. Su, S.Y. Yuan, Microbial hexachlorobenzene dechlorination under three reducing conditions, Chemosphere 36 (1998) 2721–2730.

[4] S.G. Pavlostathis, M.T. Prytula, Kinetics of the sequential microbial reductive dechlorination of hexachlorobenzene, Environ. Sci. Technol. 34 (2000) 4001–4009.
[5] F. Brahushi, U. Dörfler, R. Schroll, J.C. Munch, Stimulation of reductive dechlorination of hexachlorobenzene in soil by inducing the native microbial activity, Chemosphere 55 (2004) 1477–1484.
[6] H. Tahiri, Y.A. Ichou, J.M. Herrmann, Photocatalytic degradation of chlorobenzoic isomers in aqueous suspensions of neat and modified titania, J. Photochem. Photobiol. A 114 (1998) 219–226.
[7] K.H. Wang, Y.H. Hsieh, M.Y. Chou, C.Y. Chang, Photocatalytic degradation of 2-chloro and 2-nitrophenol by titanium dioxide suspensions in aqueous solution, Appl. Catal. B Environ. 21 (1999) 1–8.
[8] M.A. Keane, G. Pina, G. Tavoularis, The catalytic hydrodechlorination of mono-, di- and trichlorobenzenes over supported nickel, Appl. Catal. B Environ. 48 (2004) 275–286.
[9] W. Nishijima, Y. Ochi, T.Y. Tsai, Y. Nakano, M. Okada, Catalytic hydrodechlorination of chlorinated ethylenes in organic solvents at room temperature and atmospheric pressure, Appl. Catal. B Environ. 51 (2004) 135–140.
[10] H.M. Roy, C.M. Wai, T. Yuan, J.K. Kim, W.D. Marshall, Catalytic hydrodechlorination of chlorophenols in aqueous solution under mild conditions, Appl. Catal. A Gen. 271 (2004) 137–143.
[11] J. Stach, V. Pekárek, R. Endršt, J. Hetflejš, Dechlorination of hexachlorobenzene on MWI fly ash, Chemosphere 39 (1999) 2391–2399.
[12] K. Miyoshi, T. Nishio, A. Yasuhara, M. Morita, T. Shibamoto, Detoxification of hexachlorobenzene by dechlorination with potassium–sodium alloy, Chemosphere 55 (2004) 1439–1446.
[13] G. Yuan, M.A. Keane, Role of base addition in the liquid-phase hydrodechlorination of 2,4-dichlorophenol over Pd/Al_2O_3 and Pd/C, J. Catal. 225 (2004) 510–522.
[14] G.V. Lowry, M. Reinhard, Hydrodehalogenation of 1- to 3-carbon halogenated organic compounds in water using a palladium catalyst and hydrogen gas, Environ. Sci. Technol. 33 (1999) 1905–1910.
[15] G. Yuan, M.A. Keane, Liquid phase catalytic hydrodechlorination of chlorophenols at 273 K, Catal. Commun. 4 (2003) 195–201.
[16] Y. Ukisu, S. Kameoka, T. Miyadera, Catalytic dechlorination of aromatic chlorides with noble-metal catalysts under mild conditions: approach to practical use, Appl. Catal. B Environ. 27 (2000) 97–104.
[17] V. Felis, C.D. Bellefon, P. Fouilloux, D. Schweich, Hrdrodechlorination and hydrodearomatisation of monoaromatic chlorophenols into cyclohexanol on Ru/C catalysts applied to water depollution: influence of the basic solvent and kinetics of the reactions, Appl. Catal. B Environ. 20 (1999) 91–100.
[18] B.F. Hagh, D.T. Allen, Catalytic hydroprocessing of chlorinated benzenes, Chem. Eng. Sci. 45 (1990) 2695–2701.
[19] S. Krishnamoorthy, J.P. Baker, M.D. Amiridis, Catalytic oxidation of 1,2-dichlorobenzene over V_2O_5/TiO_2-based catalysts, Catal. Today 40 (1998) 39–46.
[20] S. Krishnamoorthy, M.D. Amiridis, Kinetic and in situ FTIR studies of the catalytic oxidation of 1,2-dichlorobenzene over V_2O_5/Al_2O_3 catalysts, Catal. Today 51 (1999) 203–214.
[21] S. Krishnamoorthy, J.A. Rivas, M.D. Amiridis, Catalytic oxidation of 1,2-dichlorobenzene over supported transition metal oxides, J. Catal. 193 (2000) 264–272.
[22] Y. Liu, M.F. Luo, Z.B. Wei, Q. Xin, P.L. Ying, C. Li, Catalytic oxidation of chlorobenzene on supported manganese oxide catalysts, Appl. Catal. B Environ. 29 (2001) 61–67.
[23] J. Lichtenberger, M.D. Amiridis, Catalytic oxidation of chlorinated benzenes over V_2O_5/TiO_2 catalysts, J. Catal. 223 (2004) 296–308.
[24] R.W. Van den Brink, R. Louw, P. Mulder, Formation of polychlorinated benzenes during the catalytic combustion of chlorobenzene using a $Pt/\gamma\text{-}Al_2O_3$ catalyst, Appl. Catal. B Environ. 16 (1998) 219–226.
[25] V.D. Santo, C. Dossi, S. Recchia, P.E. Colavita, G. Vlaic, R. Psaro, Carbon tetrachloride hydrodechlorination with organometallics-based platinum and palladium catalysts on MgO, J. Mol. Catal. A Chem. 182–183 (2002) 157–166.
[26] P.D. Hooker, K.J. Klabunde, Destructive adsorption of carbon tetrachloride on iron(III) oxide, Environ. Sci. Technol. 28 (1994) 1243–1247.
[27] Y.X. Li, H. Li, K.J. Klabunde, Destructive adsorption of chlorinated benzenes on ultrafine (nanoscale) particles of magnesium oxide and calcium oxide, Environ. Sci. Technol. 28 (1994) 1248–1253.
[28] R. Weber, K. Nagai, J. Nishino, H. Shiraishi, M. Ishida, T. Takasuga, K. Konndo, M. Hiraoka, Effects of selected metal oxides on the dechlorination and destruction of PCDD and PCDF, Chemosphere 46 (2002) 1247–1253.
[29] Y. Jiang, S. Decker, C. Mohs, K.J. Klabunde, Catalytic solid state reactions on the surface of nanoscale metal oxide particles, J. Catal. 180 (1998) 24–25.
[30] S.P. Decker, J.S. Klabunde, A. Khaleel, K.J. Klabunde, Catalyzed destructive adsorption of environmental toxins with nanocrystalline metal oxides. Fluoro-, chloro-, bromocarbons, sulfur, and organophosophorus compounds, Environ. Sci. Technol. 36 (2002) 762–768.
[31] I.N. Martyanov, K.J. Klabunde, Decomposition of CCl_3F over vanadium oxides and $[MgV_xO_y]MgO$ shell/core-like particles, J. Catal. 224 (2004) 340–346.